

Imbibition triggered by capillary condensation in nanopores

Olivier Vincent,^{*} Bastien Marguet, and Abraham D. Stroock^{*}

*Robert Frederick Smith School of Chemical and Biomolecular Engineering, Cornell University,
120 Olin Hall, Ithaca NY 14853*

E-mail: olivier.vincent@cornell.edu; ads10@cornell.edu

Abstract

We study the spatio-temporal dynamics of water uptake by capillary condensation from unsaturated vapor in mesoporous silicon layers (pore radius $r_p \simeq 2$ nm), taking advantage of the local changes in optical reflectance as a function of water saturation. Our experiments elucidate two qualitatively different regimes as a function of the imposed external vapor pressure: for low saturations, equilibration occurs via a diffusion-like process; for high saturations, an imbibition-like wetting front results in fast equilibration towards a fully saturated sample. We show that the imbibition dynamics can be described by a modified Lucas-Washburn equation that takes into account the liquid stresses implied by Kelvin equation.

Introduction

The interaction of porous media with liquids and vapors occurs in many contexts. In nature, water is ubiquitous within soils, rocks, or the atmosphere, and its behavior in pores is fundamental for the hydration and of plants and their vascular flows,¹ the stability of sand terrains,² and the formation of clouds by condensation on atmospheric particles.³ In technology, the permeation of liquids through porous media occurs in a diversity of applications, from printing ink on paper to oil recovery.⁴ As a result, the dynamics of invasion of a pore space when put in contact with liquid, i.e. imbibition, has been the subject of many studies, from the early work of Lucas and Washburn^{5,6} to recent work on nanoporous media.^{7,8} The observed dynamics of invasion show excellent agreement with the classical Lucas-Washburn equations, even in pores approaching the molecular size.^{9,10}

Nanopores, however, can fill with liquid even if in contact with the vapor phase only. This phenomenon, known as capillary condensation, occurs for any pore size but persists for vapor pres-

ures significantly below saturation only for diameters in the nanometer range.¹¹ Capillary condensation plays a role in many areas of science and technology such as the cohesion and friction of granular materials,¹² or the dynamics of hydrocarbons in subsurface reservoirs.¹³ Adsorption by capillary condensation, and the reverse process of desorption are still subject of active research, with outstanding questions related to the collective effects induced by disorder in the pore network^{14,15} or to deviations from macroscopic thermodynamics and dynamics at the nanoscale.^{10,16}

The experimental study of both imbibition and capillary condensation at the nanoscale is challenging due to the difficulty of accessing the local filling state of the porous medium: often only the global mass uptake can be recorded.^{17,18} Spatially resolved information can however be obtained by more sophisticated techniques such as interferometry,⁷ neutron radiography⁸ or capacitance measurements.¹⁹ Here, we use the local changes in reflectance of quasi two-dimensional, laterally connected porous silicon layers to study the dynamics of water uptake as a function of

the imposed water vapor pressure (relative humidity) around the medium. We elucidate a qualitative transition as a function of humidity from a diffusion-like regime to an imbibition-like regime. For the imbibition-like regime, we show that a modified Lucas-Washburn equation that takes into account the effective capillary pressure predicted from Kelvin-Laplace equation explains our observations quantitatively.

Methods

We formed a $5\text{ }\mu\text{m}$ thick layer of mesoporous silicon (PoSi) on top of a p-type silicon (Si) wafer of $\langle 111 \rangle$ crystal orientation and $1 - 10\Omega\cdot\text{cm}$ resistivity, by anodization in a mixture of 1:1 49% hydrofluoric acid: pure ethanol at $20\text{mA}/\text{cm}^2$ current density for 5 minutes. We then used thermal oxidation at 700°C in pure oxygen for 30 seconds to increase hydrophilicity and stabilize the porous layer. From previous studies we expect a laterally connected pore structure with porosity, $\phi = 0.45$ and a typical pore radius, $r_p = 1.5 - 2\text{ nm}$.^{10,20}

The sample resulting from these processing steps is sketched in Figure 1a. Such a sample could equilibrate quickly with the environment due to the open top surface and to the small thickness of the porous silicon layer ($\sim \mu\text{m}$). For that reason, we measured the reflectance isotherms (see below) at this step in the fabrication process. We then sealed the top surface to glass by anodic bonding (Figure 1b), so that the sample could exchange vapor only at its open edge; this change resulted in much slower equilibration dynamics in the y direction due to the large lateral dimensions of the porous layer ($\sim \text{cm}$). Figure 1c presents a top-view photograph of a sample as in Figure 1b.

We placed the sample in a vacuum chamber equipped with an optical window, thermostated at $T = 15^\circ\text{C}$ (Figure 1d). Pure water vapor, obtained by evaporation from a degassed liquid water source, flowed through the chamber towards the vacuum pump, and we measured its pressure p using a pressure gauge connected to the chamber. By adjusting the relative opening of two needle valves v_1 and v_2 , we could set the pressure between $p = 0$ and $p = p_{\text{sat}}$. All capillary condensation experiments started with a dry sample equilibrated for at

least 24 hours at $p = 0$ (v_1 closed). Opening v_1 at a time defined as $t = 0$ allowed us to impose a steady, non-zero vapor pressure p after a transient time of typically $\simeq 10$ seconds (Figure 1e). From the error of the pressure gauge reading as well as the measured fluctuations of T and p during the experiments, we estimated an uncertainty on the activity, $a = p/p_{\text{sat}}$ of ± 0.005 .

We recorded time-lapse image sequences of the sample, and analyzed its response to changes in vapor pressure by extracting the local relative change in reflectance $\Delta I/I$ under constant, white-light, diffuse illumination. From the images, we calculated $(\Delta I/I)_i = (g_i^{\text{ref}} - g_i)/g_i^{\text{ref}}$ where g_i was the grayscale value of the i^{th} pixel in the image ($g_i \in [0 - 255]$) and g_i^{ref} was its average value for $t < 0$, corresponding to the dry sample. Water uptake produced a darkening of the image, resulting in $(\Delta I/I)_i > 0$. For the measurement of the reflectance isotherm, we evaluated the average change in intensity, $\langle \Delta I/I \rangle = \frac{1}{N} \sum_i (\Delta I/I)_i$ over the whole region of interest shown in Figure 1c ($\langle \Delta I/I \rangle_{xy}$), while for the extraction of invasion dynamics propagating along y , averaging was done along the x direction only ($\langle \Delta I/I \rangle_x(y)$, axes shown in Figure 1c).

Theory

Kelvin Equation We consider liquid-vapor equilibrium at temperature T with liquid at pressure P and vapor at pressure p . It is convenient to define the activity, a , of the vapor, which compares the vapor pressure to its saturation value $p_{\text{sat}}(T)$,

$$a = \frac{p}{p_{\text{sat}}}. \quad (1)$$

Note that the quantity $a \times 100$ is also the percent relative humidity of the vapor [%RH]. Bulk equilibrium between liquid and vapor imposes $P = p = p_{\text{sat}}(T)$. In a porous medium, however, the liquid and vapor phase can coexist at different pressures due to the capillary pressure associated with the curved liquid-vapor meniscus. From Laplace equation $P - p = \sigma \mathcal{C}$, where $\mathcal{C} [\text{m}^{-1}]$ is the curvature of the meniscus and $\sigma [\text{N/m}]$ is the surface tension of the liquid. The condition for equilibrium, even with $P \neq p$, is the equality of the chem-

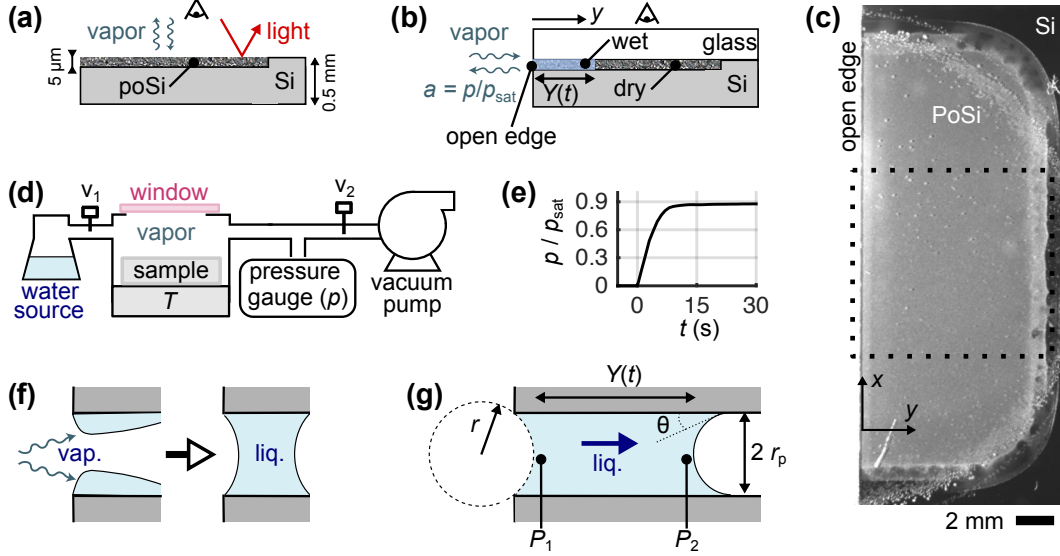


Figure 1: Side-view sketch of the sample before (a) and after (b) bonding to glass. (c) Top-view photograph of the sample. The dashed square shows the portion of the sample displayed in Figure 3a. (d) Sketch of the vacuum system used to control the vapor pressure and the temperature. (e) Vapor pressure signal during an experimental run, showing a typical early transient. (f) Schematic of the process of capillary condensation of vapor into liquid in a pore. (g) Pore-scale representation of the dynamics of liquid invasion following condensation at high vapor pressure, driven by the competition between the capillary pressures P_1 (determined by Kelvin equilibrium: Equation 2) and P_2 (determined by the geometry of the pore and the equilibrium contact angle of the liquid on the pore wall: Equation 4).

ical potentials μ_{liq} and μ_{vap} in the liquid and vapor phases. Integration of the isothermal Gibbs-Duhem equation, taking $P = p = p_{\text{sat}}$ (chemical potential μ_0) as a reference state, yields $\mu_{\text{liq}} = \mu_0 + v_m(P - p_{\text{sat}})$ and $\mu_{\text{vap}} = \mu_0 + RT \ln(a)$, where v_m is the molar volume of the liquid, and R is the universal gas constant. The expression of μ_{vap} uses the assumption that the vapor behaves as a perfect gas, while that of μ_{liq} is obtained assuming an incompressible liquid (v_m independent of pressure, which results in negligible errors for water at room temperature¹⁰). Eventually, the equilibrium condition through the equality of chemical potential requires

$$P = p_{\text{sat}} + \Psi(a) \quad (2)$$

where we have defined the vapor water potential

$$\Psi(a) = \frac{RT}{v_m} \ln(a). \quad (3)$$

Equation 2 is known as Kelvin equation, and is based on macroscopic thermodynamic considerations and descriptions of the pore fluid. Kelvin equation has however been shown to accurately

describe liquid capillary stresses due to subsaturated liquid-vapor equilibrium, even in nanoscale confinements.^{10,21,22}

Liquid invasion dynamics At high vapor pressure, it becomes thermodynamically favorable for the pores to fill with liquid by the process of capillary condensation.¹¹ Capillary condensation causes the formation of liquid plugs at the sample edge (Figure 1f), which progressively invade the whole depth of the pores. We assume that the pore filling after capillary condensation proceeds by bulk liquid flow driven by the competition of capillary pressures P_1 and P_2 as depicted in Figure 1g, and that condensation of vapor at the edge (meniscus 1) provides the liquid necessary to account for the advance of meniscus 2. In other words, we consider that the pore wetting dynamics is slow compared to the dynamics of vapor condensation at the edge,²³ so that meniscus 1 is in local thermodynamic equilibrium with the vapor. As a result, from Equations 2-3, $P_1 = \Psi(a)$, where we have neglected p_{sat} compared to Ψ . We assume

that the curvature of meniscus 2 is defined by the local mechanical equilibrium of the triple line, i.e., the curvature is $\mathcal{C} = -2\cos\theta/r_p$ where θ is the equilibrium contact angle of the liquid on the solid and r_p the radius of the pore. From Laplace equation, $P_2 - p = \Psi_c$ where

$$\Psi_c = -\frac{2\sigma\cos\theta}{r_p} \quad (4)$$

is the intrinsic capillary pressure of the pore. Neglecting the vapor pressure p compared to P_2 , we have $P_2 = \Psi_c$ and

$$\Delta P = P_1 - P_2 = \Psi(a) - \Psi_c. \quad (5)$$

The driving force for the flow is the pressure gradient $\nabla P = \Delta P/Y(t)$, where $Y(t)$ is the location of meniscus 2 (Figure 1g). We describe the flow response to that gradient using Darcy equation $q = \rho_{\text{liq}}\kappa\nabla P$, where q [kg/(m².s)] is the mass flux, ρ_{liq} is the density of the liquid, and κ [m²/(Pa.s)] is the permeability of the porous layer. Using the conservation of mass $q = \rho_{\text{liq}}\phi dY/dt$, the front position $Y(t)$ obeys the differential equation $YdY/dt = \kappa\Delta P/\phi$. Integration using $Y = 0$ at $t = 0$ yields

$$\frac{Y^2(t)}{t} = w = \frac{2\kappa}{\phi}(\Psi(a) - \Psi_c) \quad (6)$$

where we have used Equation 5 to express the pressure difference ΔP . When $\Psi(a) = 0$ (i.e. $p = p_{\text{sat}}$ from Equations 1 and 3), Equation 6 reduces to the Lucas-Washburn law for the dynamics of imbibition, which describes the non-inertial dynamics of liquid invasion when the sample edge is plunged in bulk liquid.²⁴ The extra term $\Psi(a)$ accounts for the existence of an additional capillary pressure governed by Kelvin equation when the sample is in contact with vapor instead of liquid (Figure 1g). We will refer to the parameter w as the *imbibition speed coefficient* in the rest of the paper.

Vapor invasion dynamics At low vapor pressures, no capillary condensation occurs, but vapor can adsorb on the pore walls. The average density $\rho(a)$ inside of the pore depends on the vapor activity, and varies between $\rho = 0$ at $a = 0$ (evacuated sample) to $\rho = \rho_{\text{liq}}$, as a approaches

1 (pore filled with liquid of density ρ_{liq} due to capillary condensation). It is thus convenient to define $\alpha(a) = \rho(a)/\rho_{\text{liq}}$, which takes values between 0 and 1. The dynamics of vapor invasion in the pores is a result of the combined effects of transport through the pores and adsorption on the pore walls, and obeys the conservation of mass $\partial q/\partial y = -\phi\partial\rho/\partial t$. We define a generic transport coefficient $k(a)$ so that $q = -\phi\rho_{\text{liq}}k(a)\partial a/\partial y$; the conservation of mass then translates into

$$\alpha'\frac{\partial a}{\partial t} = \frac{\partial}{\partial y}\left(k(a)\frac{\partial a}{\partial y}\right), \quad (7)$$

where we have defined $\alpha' = d\alpha/da$ the derivative of the adsorption function. Equation 7 is a complex diffusion equation with activity-dependent coefficients, but for small variations in activity, it reduces to a simple diffusion equation with an effective diffusivity

$$D = \frac{k}{\alpha'}. \quad (8)$$

Equation 8 illustrates the competition between transport and adsorption: when the adsorbed mass changes rapidly as a function of vapor pressure (α' large), adsorption on the pore walls act as a sink, slowing down the propagation of the vapor. Equations 7-8 are very general and will serve as a basis for discussion of the possible mechanisms that are at play during equilibration of the samples with vapor.

The generic transport parameter k incorporates the physics of transport. If transport is dominated by diffusion in the vapor phase, by Fick's law we have $q = \phi MD_m/\tau \times \partial C/\partial y$, where D_m is the molecular diffusivity, M is the molar mass, and $C = p/(RT)$ is the concentration, assuming that the vapor behaves as an ideal gas, and τ is the tortuosity of the pore space. The transport coefficient is then $k = D_m p_{\text{sat}} v_m / (\tau RT)$. In nanometer-size pores, the diffusivity can be estimated as $D_m = (2r_p/3)\sqrt{8RT/(\pi M)}$ from Knudsen diffusion,²⁵ yielding $D_m \simeq 8 \times 10^{-7}$ m²/s for water vapor in pores 2nm in radius, corresponding to a transport coefficient $k \simeq 2 \times 10^{-12}$ m²/s. Assuming $\alpha' \sim 1$ for typical adsorption isotherms, we expect D to also be on the order of 10^{-12} m²/s if transport is based on Knudsen diffusion. This value will serve

as a reference in our discussion of the diffusion mechanisms below.

Results

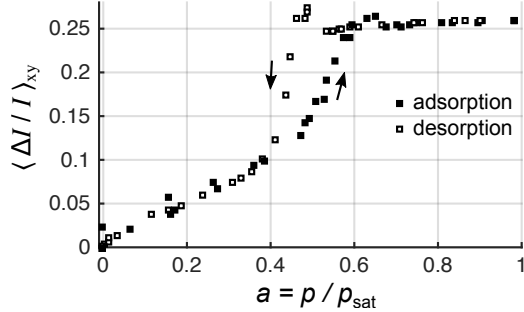


Figure 2: Reflectance isotherm of the sample measured on the open sample (Figure 1a). $\langle \Delta I / I \rangle_{xy}$ represents the relative change in average grayscale intensity with respect to the dry sample (see Methods). $\langle \Delta I / I \rangle_{xy} > 0$ corresponds to a darker image and to a higher sample saturation.

Reflectance isotherm We first recorded the static changes in reflectance of the porous silicon layer as a function of the vapor activity $a = p/p_{\text{sat}}$ with an open sample (not bonded to glass) as sketched in Figure 1a. The resulting *reflectance isotherm* is presented in Figure 2. These reflectance isotherms display features characteristic of adsorption and desorption isotherms measured by mass in nanoporous media:¹¹ a reversible plateau at high relative humidities (here for $a > 0.65$), associated with the presence of bulk liquid in all the pores; a reversible branch at low relative humidities (here for $a < 0.4$), associated with the presence of adsorbed molecules on the pore walls; and a hysteresis loop at intermediate relative humidities, with desorption occurring at lower pressure than adsorption. Although the nature of the hysteresis loop and its relationship to pore structure are still debated, the adsorption branch is typically interpreted as the result of capillary condensation.^{9,11}

The close resemblance between the reflectance isotherm and mass isotherms for water in porous silicon²⁶ suggests that there is a direct, close-to-linear relationship between adsorbed mass and reflectance, and thus that studying optical changes is

a useful tool to access local concentration changes during dynamic experiments. Compared to a mass isotherm, we note additional features. In particular, "spikes" stand out above the hysteresis loop at the edge of desorption (for a slightly below 0.5) and in the later stages of capillary condensation (for $a \simeq 0.6 - 0.65$). We interpret the presence of these spikes as a loss of reflectance associated with increased light diffusion in the porous medium due to the formation of large clusters of liquid and vapor of size comparable to the wavelength of light. Such effects have been reported in Vycor porous glass both for light and sound propagation.^{27,28}

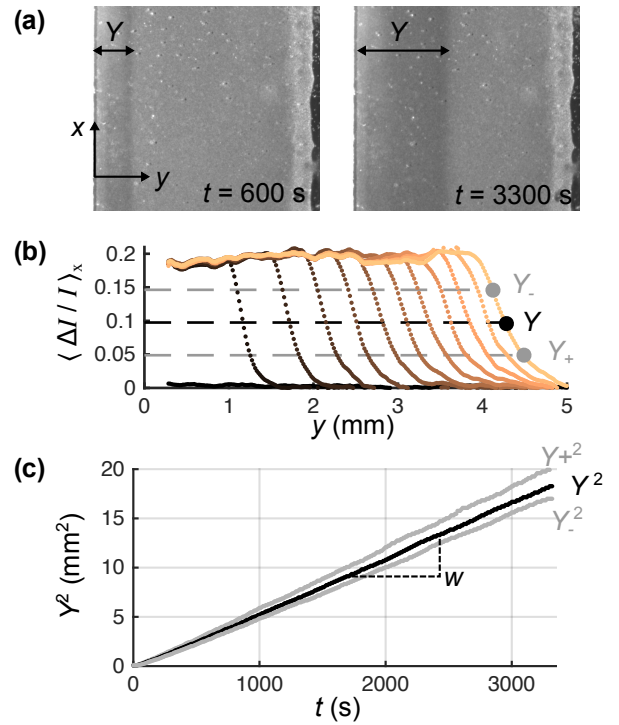


Figure 3: Imbibition by capillary condensation at high relative humidities ($a > 0.6$), here for $a = 0.98$. (a) Raw images obtained during the experiment (the field of view is that defined in Figure 1c). (b) Results of image analysis showing the reflectance change as a function of position. Colors represent different times, starting from $t = 0$ (black points around $\Delta I / I = 0$) and with a time separation of 5 min. The horizontal dashed lines show how the front position is extracted from the data. (c) Front position squared as a function of time.

Invasion dynamics We then recorded dynamics change in reflectance with the sample bonded to glass such as depicted in Figure 1b, during equili-

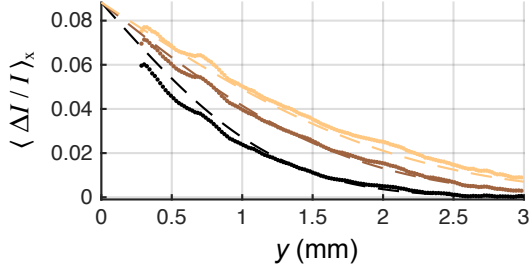


Figure 4: Diffusion-like dynamics at low relative humidities ($a < 0.6$), here for $a = 0.50$. Colors represent different times of 40 min, 80 min and 120 min after the beginning of the experiment. The dashed lines are solutions of the diffusion equation, with a constant diffusivity $D = 2 \times 10^{-10} \text{ m}^2/\text{s}$.

bration with a vapor of constant activity $a = p/p_{\text{sat}}$ after complete evacuation. In such a configuration, exchange of mass was only possible at the open edge (left) of the sample, and we monitored, optically, the resulting lateral propagation of changes in reflectance.

At high imposed relative humidities ($a > 0.6$), the equilibration process resulted in a clearly visible invasion front propagating away from the open edge (Figure 3a). Image analysis allowed us to extract the front profile as a function of time, after averaging over the x direction. The resulting data (Figure 3b) showed the propagation of a sharp front separating a fully wet zone (to the left, $\langle \Delta I / I \rangle_x \simeq 0.2$) from a dry zone (to the right, $\langle \Delta I / I \rangle_x = 0$). Note that the fully wet intensity was lower than that on the reflectance isotherm (0.20 vs. 0.26) due to the presence of the glass layer on top of the porous silicon layer. We quantified the front propagation by extracting the mean front position $Y(t)$ and estimated its width using Y_+ and Y_- (see Figure 3b). As shown in Figure 3c, the three parameters, Y , Y_+ and Y_- , exhibited a \sqrt{t} scaling, typical of imbibition dynamics.^{9,24}

For lower imposed vapor pressures ($a < 0.6$), the equilibration dynamics was qualitatively different, with a diffusion-like penetration of moisture into the sample rather than a well-defined front (Figure 4). Quantitatively, the dynamics was also much slower, as shown by the very different timescales in Figures 3b and 4.

We performed a series of experiments in the imbibition-like regime ($a > 0.6$), at different im-

posed vapor activities, a , or equivalently different vapor water potentials $\Psi(a)$ from Equation 3. Using linear fits of the data as in Figure 3, we extracted the imbibition speed coefficient $w = Y^2/t$ and a typical front width $\Delta w = w_+ - w_-$ with $w_+ = Y_+^2/t$ and $w_- = Y_-^2/t$ as a function of $\Psi(a)$. The results are shown in Figure 5 and demonstrate a linear decrease in the imbibition speed as Ψ becomes more negative, as well as a front width that is weakly dependent on the imposed vapor activity.

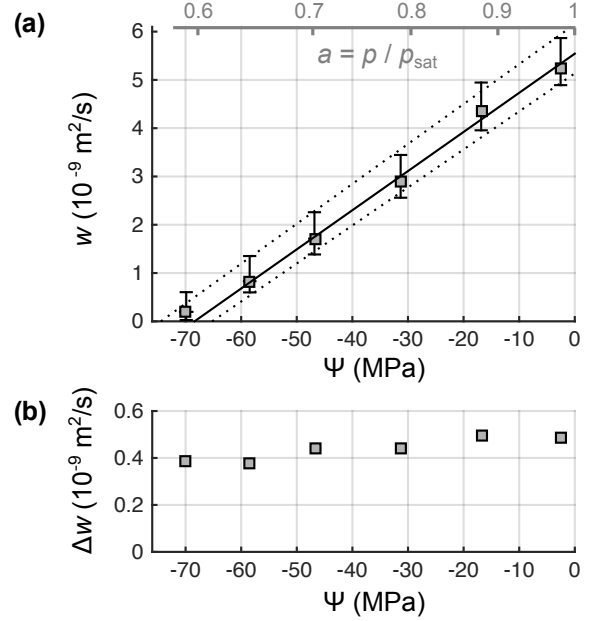


Figure 5: Front properties for imbibition-like dynamics at high imposed vapor activities ($a > 0.6$). (a) Imbibition speed coefficient, w , as a function of the Kelvin water potential $\Psi(a)$ (bottom axis) calculated from the activity a (top axis) with Equation 3. Values of w were extracted from experiments such as those in Figure 3, as the slope of the $Y^2(t)$ data in Figure 3c. The error bars were obtained from the values w_- and w_+ estimated from Y_- and Y_+ , respectively. The lines are linear fits of w , w_- and w_+ . (b) Imbibition front width, $\Delta w = w_+ - w_-$, as a function of water potential.

Discussion

In all the experiments reported above (Figures 3 - 5), we started with the sample in a dry state ($a = 0$), and the equilibration with a vapor at $a > 0$ resulted in moisture uptake in the pores. As a result, the processes involved in the dynamics relate

to the adsorption branch of the isotherm. From the reflectance isotherm of Figure 2, it is clear that the value $a = 0.6$ marked a transition: for $a > 0.6$, capillary condensation resulted in complete filling of all the pores, while for $a < 0.6$ the sample was only partially saturated. Consequently, it is reasonable to assume that in dynamic situations, imposing $a > 0.6$ resulted in the saturation with liquid of the pores at the sample edge, similarly to what would happen if the sample were directly dipped in the bulk liquid, a case classically described with Lucas-Washburn dynamics. Here, however, the samples were not in contact with bulk liquid but with a subsaturated vapor; in this scenario, we expect that an additional meniscus exists at the open end of the pore, as depicted in Figure 1g. The driving force for the liquid flow thus resulted from the competition of the capillary pressure of two menisci – one at the open edge and the other at the advancing front (Figure 1g) – leading to the modified Lucas-Washburn dynamics expressed in Equation 6, with a natural driving force proportional to $\Psi(a) - \Psi_c$; $\Psi(a)$ represents the capillary pressure imposed by the local liquid-vapor Kelvin equilibrium (Equation 2) at the sample edge, while Ψ_c represents the intrinsic capillary pressure associated with the pore geometry and wetting properties (Equation 4). The classical Washburn relation is recovered in the limit $a \rightarrow 1$, i.e. when the vapor approaches saturation; our model thus predicts that imbibition dynamics is identical when using saturated vapor and when using bulk liquid as the boundary condition at the sample edge.

Experimental results as in Figure 5a show excellent agreement with the linear $w(\Psi)$ dependence predicted by Equation 6. Furthermore, the $w = 0$ intercept and the slope of the linear fits in Figure 5a allows us to estimate from Equation 6 both the intrinsic capillary pressure $\Psi_c = -70 \pm 5$ MPa and the Darcy permeability of the porous layer $\kappa = 1.82 \pm 0.05 \text{ m}^2/(\text{Pa.s})$ independently, using $\phi = 0.45$.¹⁰ These values are almost identical to those obtained from drying-induced permeation experiments on similar porous silicon layers that we reported recently.¹⁰ This excellent agreement validates our interpretation of the imbibition-like dynamics and the applicability of the modified Lucas-Washburn equation that takes into account the Kelvin capillary pressure (Equation 6);

it also suggests that our assumption that the optical signal, $\Delta I/I$, reflects the local mass uptake in the medium was appropriate.

The success of this modified Lucas-Washburn treatment (Equation 6 applied to Figure 5a) indicates that imbibition from a saturated vapor ($a = 1$, $\Psi = 0$) is equivalent to imbibition from bulk liquid, when local equilibrium at the exposed edge is ensured. This equivalence has been debated in the membrane science community under the name "Schroeder's paradox", based on observation of distinct absorption properties from pure liquid and saturated vapor in swelling media.^{29,30} Neuman and colleagues have provided an explanation of this effect as arising from history-dependent properties of certain materials (e.g. Nafion).³¹ For rigid membranes with well-defined pore structure, such as the porous silicon studied here, our observations support the expectation that imbibition dynamics should be defined by the chemical potential at the boundary, independent of the phase that imposes this boundary state.

Classical Lucas-Washburn imbibition experiments in bulk liquids only provide a measure of the product $\kappa \times \Psi_c$,^{18,24} except if the pressure P of the liquid reservoir in contact with the sample can be varied: in this latter case, the $w(P)$ response allows the estimation of κ and Ψ_c separately, but requires the use of large positive pressures of magnitude comparable to Ψ_c .³² The technique proposed here uses a similar strategy, but the pressure at the edge is brought to large, *negative* values, taking advantage of the fact that small changes in vapor activity result in large changes in the Kelvin stress (Equation 2). We recently reported another method exploiting Kelvin stresses to measure both κ and Ψ_c , using drying-induced, steady-state permeation flows.¹⁰ Globally, using vapor-liquid equilibrium provides a convenient way to vary the capillary stress in the pore liquid (i.e. the driving force for the flow) in a continuous manner through Kelvin equation.

The parameters κ and Ψ_c are associated with the viscous drag in the pores and with capillary effects, respectively, and their measurement offers an interesting way to probe the fluid mechanics of confined liquids. As we have discussed recently,¹⁰ the measured values of κ and Ψ_c suggest that the fluidity and capillarity of water are not no-

ticeably modified in nanoscale confinements: using Laplace law of capillarity (Equation 4) with $\theta = 25 \pm 5^\circ$ and the bulk surface tension of water $\sigma = 0.073 \text{ N/m}$,^{10,26} we estimate a pore size of $r_p = 1.9 \pm 0.2 \text{ nm}$, compatible with pore size estimates using Kelvin-Laplace equation on the reflectance isotherm obtained here ($r_p = 1.8 \pm 0.5 \text{ nm}$),³³ or BJH analysis from N_2 mass isotherms ($r_p = 1.4 \pm 0.4 \text{ nm}$) and dynamic permeation flow measurements ($r_p = 1.7 \pm 0.2 \text{ nm}$) obtained on a separate sample.¹⁰ The pore size value of $r_p = 1.9 \pm 0.2 \text{ nm}$ is also compatible with the Carman-Kozeny relation $\kappa = \phi r_{\text{eff}}^2 / (8\eta\tau)$ using the bulk water viscosity $\eta = 1.14 \times 10^{-3} \text{ Pa.s}$, the tortuosity of the porous layer $\tau = 4.5$, and an effective hydraulic radius $r_{\text{eff}} = r_p (1 - d/r_p)^2$ that accounts for the immobility of one monolayer of thickness $d = 0.31 \text{ nm}$ at the pore wall.¹⁰ This consistency, as well as the compatibility of the observed imbibition dynamics with the stresses predicted from Kelvin equation, provide another demonstration of the excellent extension of the macroscopic laws of capillarity, viscous flow, and thermodynamics at the nanoscale.^{10,18}

According to Equation 6, when the external vapor activity a is low enough such that $\Psi(a) = \Psi_c$, there is no net capillary force driving bulk liquid flow. From Equation 2, $\Psi(a) = \Psi_c$ with the value of Ψ_c determined above corresponds to $a = 0.59 \pm 0.02$, in accordance with the experimentally observed transition to a diffusion-like regime below $a \simeq 0.6$. In the diffusion-like regime, while there is no capillary driving force for equilibration, there is a chemical potential driving force, as the dry sample needs to uptake some water to come to equilibrium (see Figure 2). As a result of this chemical potential imbalance, mass diffusion occurs through the porous medium, explaining the diffusion-like dynamics below $a = 0.6$.

We estimated the effective diffusivity in that regime by fitting the data as in Figure 4 with analytical solutions of the one-dimensional diffusion equation with constant diffusivity D .³⁴ We note that the diffusivity in Equation 7 is not constant a priori, so the simple fitting with a constant D only provides a way to discuss order of magnitudes. As can be seen in Figure 4, the hypothesis of a constant diffusivity fits the data reasonably well. The diffusivity obtained from the fit was sim-

ilar ($D \simeq 2 \times 10^{-10} \text{ m}^2/\text{s}$) for two experiments in the diffusion-like regime, one below the hysteresis cycle ($a = 0.35$) and one in the capillary condensation regime ($a = 0.50$). This value may seem low compared to typical bulk molecular diffusivities, but D is in fact not a true molecular diffusivity, but rather incorporates effects from both transport coefficients in the porous medium and local adsorption thermodynamics. Indeed, molecules uptaken in the pores are either adsorbed locally, or transported further in the medium, as illustrated by Equation 8. Based on Knudsen diffusion, Equation 8 however predicts D two orders of magnitude smaller than the experimental value (see Theory). This disagreement suggests that surface transport in the adsorbed water at the pore walls may play an important role in the diffusion dynamics. In fact the observed value of D is typical of that reported for surface flows in porous glass and porous silicon.³⁵

Regardless of the physical mechanism behind the effective diffusion process, we note that both the imbibition-like regime and the diffusion-like regime result in invasion dynamics scaling as \sqrt{t} , resulting in equilibration times $\tau \sim L^2/w$ and $\tau \sim L^2/D$ respectively, for a sample of dimension L . As w and D are separated by more than an order of magnitude, equilibration in the imbibition-like regime is much more efficient than in the diffusion-like regime. Also, since both processes display the same qualitative dynamics $\propto \sqrt{t}$, global mass uptake experiments are not able to distinguish between them, and only spatially resolved measurements as presented here can unveil their contributions.

Finally, we comment on the width of the imbibition-like front (Figures 3c and 5b): since both Y_+ and Y_- scaled as \sqrt{t} (Figure 3c), the widening of the imbibition front $\Delta Y = Y_+ - Y_-$ also followed a \sqrt{t} scaling. The quantity $\Delta w = w_+ - w_- = (Y_+^2 - Y_-^2)/t$ is a measure of that widening; as can be seen in Figure 5b, Δw was nearly independent of the imposed water potential and thus also insensitive to the imbibition speed in our experiments. A $t^{1/2}$ scaling for front broadening during an imbibition process is considered anomalous,⁴ but has been reported recently in nanoporous glass;⁸ these authors suggested that the anomalous broadening was due to uncorre-

lated menisci movement during imbibition when the pores are sufficiently long compared to the spacing of lateral connections. Due to limited information about the local structure and connectivity of porous silicon $\langle 111 \rangle$ layers, it is unclear if the pores in our study satisfies these geometrical conditions or if the anomalous front broadening originates from other physics.

Conclusion

We have used the optical signature induced by the uptake of water in a model nanoporous medium to study the dynamics of invasion by capillary condensation in the nanopores as a function of the imposed vapor pressure. In a broad ranges of high vapor pressures, invasion occurred as a well defined front reminiscent of Lucas-Washburn imbibition dynamics, with an additional contribution to the capillary force driving the flow that we have shown to be well described by Kelvin equation. At lower vapor pressures, moisture transport transitioned to a slower diffusion-like behavior due to the vanishing of the net capillary driving force. Both processes (imbibition and diffusion) resulted in mass uptake proportional to \sqrt{t} , but with qualitatively different spatio-temporal dynamics, as well as order-of-magnitude difference in timescales. Our analysis also suggested that imbibition from saturated vapor was equivalent to imbibition from bulk liquid, due to the insensitivity of the dynamics to the external phase in contact with the pores.

The vapor pressure dependence of the flow in the imbibition regime offers a way to finely tune the imbibition speed through the Kelvin-induced capillary pressure. This control over the dynamics by using an external, easily tunable parameter (the relative humidity of the vapor) is interesting for both fundamental studies of thermodynamics and dynamics in porous media, and for the development of technologies using the response of materials to humidity changes. For fundamental aspects, we have shown that the imbibition-like response allows an independent measurement of both the intrinsic capillary pressure and of the permeability of the porous medium, providing useful information about the capillary and viscous effects

at the nanoscale, respectively; globally, our results also demonstrate the validity of Kelvin equation in pores only $\simeq 4$ nm in diameter. For applications in, for example, sensing and membrane processes, our observations and analysis provide a robust basis for the design of materials at the pore-scale to control imbibition dynamics.

Acknowledgement The authors thank Glenn Swan for technical support and Antoine Robin for help in building the vacuum system. This work was supported by the National Science Foundation (IIP-1500261), the Air Force Office of Scientific Research (FA9550-15-1-0052), the U.S. Department of Agriculture (2015-67021-22844) and the Camille Dreyfus Teacher-Scholar Awards program, and was performed in part at the Cornell NanoScale Facility, a member of the National Nanotechnology Infrastructure Network (National Science Foundation; Grand No. ECCS-15420819).

References

- (1) Stroock, A. D.; Pagay, V. V.; Zwierniecki, M. A.; Holbrook, N. M. The Physicochemical Hydrodynamics of Vascular Plants. *Annu. Rev. Fluid Mech.* **2014**, *46*, 615–642.
- (2) Kudrolli, A. Granular matter: sticky sand. *Nature materials* **2008**, *7*, 174–175.
- (3) Marcolli, C. Deposition nucleation viewed as homogeneous or immersion freezing in pores and cavities. *Atmospheric Chemistry and Physics* **2014**, *14*, 2071–2104.
- (4) Alava, M.; Dubé, M.; Rost, M. Imbibition in disordered media. *Advances in Physics* **2004**, *53*, 83–175.
- (5) Lucas, R. Ueber das Zeitgesetz des kapillaren Aufstiegs von Flüssigkeiten. *Kolloid-Zeitschrift* **1918**, *23*, 15–22.
- (6) Washburn, E. W. The Dynamics of Capillary Flow. *Phys. Rev.* **1921**, *17*, 273–283.
- (7) Acquaroli, L. N.; Urteaga, R.; Berli, C. L. A.; Koropecski, R. R. Capillary Filling in Nanostructured Porous Silicon. *Langmuir* **2011**, *27*, 2067–2072.

- (8) Gruener, S.; Sadjadi, Z.; Hermes, H. E.; Kityk, A. V.; Knorr, K.; Egelhaaf, S. U.; Rieger, H.; Huber, P. Anomalous front broadening during spontaneous imbibition in a matrix with elongated pores. *Proceedings of the National Academy of Sciences* **2012**, *109*, 10245–10250.
- (9) Huber, P. Soft matter in hard confinement: phase transition thermodynamics, structure, texture, diffusion and flow in nanoporous media. *Journal of Physics: Condensed Matter* **2015**, *27*, 103102.
- (10) Vincent, O.; Szenicer, A.; Stroock, A. D. Capillarity-driven flows at the continuum limit. *Soft Matter* **2016**, *12*, 6656–6661.
- (11) Charlaix, E.; Ciccotti, M. In *Handbook of Nanophysics: Principles and methods*; Sattler, K., Ed.; CRC Press, 2010; Chapter Capillary condensation in confined media, pp 12.1–12.17.
- (12) Bocquet, L.; Charlaix, E.; Ciliberto, S.; Crasous, J. Moisture-induced ageing in granular media and the kinetics of capillary condensation. *Nature* **1998**, *396*, 735–737.
- (13) Barsotti, E.; Tan, S. P.; Saraji, S.; Piri, M.; Chen, J.-H. A review on capillary condensation in nanoporous media: Implications for hydrocarbon recovery from tight reservoirs. *Fuel* **2016**, *184*, 344–361.
- (14) Wallacher, D.; Künzner, N.; Kovalev, D.; Knorr, N.; Knorr, K. Capillary Condensation in Linear Mesopores of Different Shape. *Phys. Rev. Lett.* **2004**, *92*, 195704.
- (15) Aubry, G. J.; Bonnet, F.; Melich, M.; Guyon, L.; Spathis, P.; Despetis, F.; Wolf, P.-E. Condensation of helium in aerogel and athermal dynamics of the random-field ising model. *Physical review letters* **2014**, *113*, 085301.
- (16) Neimark, A. V.; Ravikovitch, P. I.; Vishnyakov, A. Bridging scales from molecular simulations to classical thermodynamics: density functional theory of capillary condensation in nanopores. *Journal of Physics: Condensed Matter* **2003**, *15*, 347.
- (17) Valiullin, R.; Naumov, S.; Galvosas, P.; Kärger, J.; Woo, H.-J.; Porcheron, F.; Monson, P. A. Exploration of molecular dynamics during transient sorption of fluids in mesoporous materials. *Nature* **2006**, *443*, 965–968.
- (18) Gruener, S.; Hofmann, T.; Wallacher, D.; Kityk, A. V.; Huber, P. Capillary rise of water in hydrophilic nanopores. *Phys. Rev. E* **2009**, *79*, 067301.
- (19) Kiepsch, S.; Pelster, R. Interplay of vapor adsorption and liquid imbibition in nanoporous Vycor glass. *Physical Review E* **2016**, *93*, 043128.
- (20) Vincent, O.; Sessoms, D. A.; Huber, E. J.; Guioth, J.; Stroock, A. D. Drying by Cavitation and Poroelastic Relaxations in Porous Media with Macroscopic Pores Connected by Nanoscale Throats. *Phys. Rev. Lett.* **2014**, *113*, 134501.
- (21) Fisher, L.; Israelachvili, J. Determination of the capillary pressure in menisci of molecular dimensions. *Chemical Physics Letters* **1980**, *76*, 325–328.
- (22) Gor, G. Y.; Bertinetti, L.; Bernstein, N.; Hofmann, T.; Fratzl, P.; Huber, P. Elastic response of mesoporous silicon to capillary pressures in the pores. *Applied Physics Letters* **2015**, *106*, 261901.
- (23) The imbibition mass flux $(\phi \rho_{\text{liq}}/2) \sqrt{w/t}$ can be compared to a typical condensation flux obtained from the kinetic theory of gases $p \sqrt{\rho_{\text{liq}} v_m / (2\pi RT)}$, which is much greater than the imbibition flux as long as $t \gg 10^{-3}$ seconds, using typical values corresponding to our experiments.
- (24) Masoodi, R., Pillai, K. M., Eds. *Wicking in Porous Materials: Traditional and Modern Modeling Approaches*; CRC Press, 2013.

- (25) Gruener, S.; Huber, P. Knudsen Diffusion in Silicon Nanochannels. *Phys. Rev. Lett.* **2008**, *100*, 064502.
- (26) Kovacs, A.; Meister, D.; Mescheder, U. Investigation of humidity adsorption in porous silicon layers. *Physica Status Solidi (a)* **2009**, *206*, 1343–1347.
- (27) Page, J.; Liu, J.; Abeles, B.; Deckman, H.; Weitz, D. Pore-space correlations in capillary condensation in Vycor. *Physical review letters* **1993**, *71*, 1216.
- (28) Soprunyuk, V. P.; Wallacher, D.; Huber, P.; Knorr, K.; Kityk, A. V. Freezing and melting of Ar in mesopores studied by optical transmission. *Physical Review B* **2003**, *67*, 144105.
- (29) Choi, P.; Datta, R. Sorption in Proton-Exchange Membranes An Explanation of Schroeder's Paradox. *Journal of the Electrochemical Society* **2003**, *150*, E601–E607.
- (30) Vallieres, C.; Winkelmann, D.; Roizard, D.; Favre, E.; Scharfer, P.; Kind, M. On Schroeder's paradox. *Journal of membrane science* **2006**, *278*, 357–364.
- (31) Onishi, L. M.; Prausnitz, J. M.; Newman, J. Water-nafion equilibria. Absence of Schroeder's paradox. *The Journal of Physical Chemistry B* **2007**, *111*, 10166–10173.
- (32) Li, L.; Kazoe, Y.; Mawatari, K.; Sugii, Y.; Kitamori, T. Viscosity and wetting property of water confined in extended nanospace simultaneously measured from highly-pressurized meniscus motion. *The journal of physical chemistry letters* **2012**, *3*, 2447–2452.
- (33) Kelvin-Laplace equation $r_p = 2\sigma v_m \cos \theta / [RT \ln(a^*)]$ combines Kelvin equation and Laplace equation to relate the pore size to the activity a^* of the confined liquid-vapor phase transition.¹¹ Considering that a^* is located in the activity range 0.45–0.65 of the reflectance isotherm hysteresis, $r_p = 1.8 \pm 0.5$ nm.
- (34) Crank, J. *The mathematics of diffusion*; Oxford University Press, 1979.
- (35) Dvoyashkin, M.; Khokhlov, A.; Naumov, S.; Valiullin, R. Pulsed field gradient NMR study of surface diffusion in mesoporous adsorbents. *Microporous and Mesoporous Materials* **2009**, *125*, 58–62.